ASM Sc. J., 21(1), 2026

https://doi.org/10.32802/asmscj.2026.0351

Optimising Calcium Titanate Doping in Bi-Free ZnO Varistor Ceramics for Low-Voltage Protection

A.M.A.A.M. Suhaimi[1], N.A.M. Nasir[1], W.M.I.W.M. Kamaruzzaman[1], M.S. Shaifudin[1], N.H.M. Daud[1,2] and M.S.M. Ghazali[1*]

[1]*Faculty of Science and Marine Environment, Universiti Malaysia Terengganu, 21030, Kuala Nerus, Terengganu, Malaysia*

[2]*Centre for Pre-University Studies, Universiti Malaysia Sarawak, 94300, Kota Samarahan, Sarawak, Malaysia*

This study systematically investigates the effects of calcium titanate (CTO) concentration on the microstructure and electrical properties of ZnO-based varistor ceramics to identify optimal Bi-free formulations for low-voltage protection applications. CTO, a perovskite oxide, was incorporated to address the volatility and environmental limitations of conventional Bi_2O_3-based varistors. Analyses of microstructural and crystallographic data reveal that low CTO concentrations promote grain growth, while higher amounts induce moderate grain refinement and increased micro-strain. Electrical characterisation demonstrates enhanced nonlinearity in all CTO-doped ZnO ceramics, with the maximum nonlinearity coefficient (α = 3.850) and lowest leakage current density (425.11 $\mu A/cm^2$) observed at 1.0 mol% CTO. The study identifies an optimal CTO concentration window that yields a balanced combination of large grain size, high potential barrier height, and stable non-ohmic response. These findings confirm CTO as an effective, thermally stable substitute for Bi_2O_3 in tailoring grain boundary properties and electrical performance, laying the groundwork for environmentally friendly ZnO varistor development. Future research should further refine doping strategies to maximise nonlinear characteristics and device reliability.

Keywords: zinc oxide varistor; calcium titanate doping; grain boundary; nonlinear electrical properties; Bi-free ceramics

I. INTRODUCTION

Zinc oxide (ZnO) varistor ceramics are the cornerstone of overvoltage protection devices, exhibiting highly nonlinear current-voltage characteristics arising from the formation of Double Schottky Barriers (DSBs) at grain boundaries (GBs) (Yang *et al.*, 2025). Low-voltage varistors are indispensable components for effective surge protection in modern integrated circuits, compact consumer electronics, and sensitive digital systems. These applications necessitate highly stable, nonlinear performance with a very low nominal breakdown voltage (V_B), typically requiring voltages below 100 V/mm (He, 2019). The cumulative behaviour of the Double Schottky Barriers (DSB) that form at the interface between semiconducting grains and the insulating, additive-rich grain boundary phases governs the fundamental electrical characteristics of a varistor (Hembram *et al.*, 2021; Lan *et al.*, 2025). The industry-standard formulation relies heavily on bismuth oxide (Bi_2O_3) as the critical additive for varistor formation. Despite its functional importance, the system presents several well-documented drawbacks related to long-term stability and high processing costs (Lungu, 2023; Malaoui *et al.*, 2025). A major disadvantage is the significant volatility at high sintering temperatures, often exceeding 1200 °C. If special sealed sintering conditions are not employed, this volatilisation leads to compositional shifts and the formation of undesirable, unstable grain boundary layers (Peiteado *et al.*, 2005).

Recent efforts have explored perovskite-type oxides, rare-earth elements, and transition-metal additives as potential substitutes for Bi_2O_3, aiming to stabilise grain boundaries,

*Corresponding author: mohdsabri@umt.edu.my

control microstructure, and improve nonlinear performance without the drawbacks of bismuth (Shaifudin, 2019). Nevertheless, research on Bi-free formulations for low-voltage ZnO varistors remains limited, and a clear understanding of the role of alternative dopants in governing grain boundary barrier formation and electrical characteristics is still lacking. Addressing this gap is crucial for designing next-generation varistors that combine enhanced nonlinearity, low leakage, and long-term stability with environmentally friendly compositions. Among the various strategies, single-doping approaches have attracted interest due to their simplicity and ability to isolate the specific effects of individual dopants on microstructural evolution and electrical performance (Fauzana *et al.*, 2013). Notably, the introduction of perovskite-related additives has provided remarkable features that reduce the number of elements or compounds within the varistor system without sacrificing its functionality, using ZnO-based varistor ceramics.

Calcium titanate (CTO), a perovskite ceramic, is proposed as a potential substitute for Bi_2O_3, primarily due to its inherent thermal stability. As a non-volatile, high-melting-point inorganic compound, it offers low cost and environmental friendliness, which fundamentally addresses the thermal aging and volatilisation issues associated with Bi_2O_3 (Shahraki *et al.*, 2019; Tian *et al.*, 2021). CTO primarily influences the DSB characteristics through solid-state reaction and segregation mechanisms. The key objective of this replacement strategy is to achieve comparable varistor performance while simultaneously stabilising grain density. However, excessive CTO will over-refine the grain structure, resulting in an excessively high breakdown voltage that is unsuitable for low-voltage protection, as its efficacy is highly dependent on its concentration (Prachamon *et al.*, 2023). Therefore, this paper aims to systematically study and synthesise the findings concerning the impact of CTO concentration on the microstructure and electrical properties of varistor ceramics, with a specific focus on defining the optimal CTO concentration regime that balances the requirement for large grain size with maximising electrical stability for low-voltage applications.

II. MATERIALS AND METHODS

ZnO-CTO-based varistors of the composition (100.0 – x) mol% ZnO + (x) mol% CTO (x = 0.0, 0.2, 0.4, 0.6, 0.8, and 1.0) were prepared by the traditional oxides mixing method utilising research-grade powders of >99.0% purity. The raw materials were mixed using the high-energy ball milling technique for two hours at milling speed of 100 rpm using stainless steel balls at a ball-to-powder weight ratio of 4:1. Then, the powder mixture was dried in a conventional laboratory oven for 120 minutes with the drying temperature was set at 80 °C after the 1.75 wt.% binder solution of polyvinyl alcohol (PVA) was added. The dried mixture was ground using a porcelain agate mortar and pestle, and sieved using a 75 µm sieve to obtain fine kick-off powder. A small amount of sieved powder was pressed using a hydraulic press machine with a 10 mm diameter under a uniaxial pressure of 2.6 T/cm², resulting in a thickness of 2.0 mm. The green pellets were subsequently sintered in air at a temperature of 1250 °C for 90 minutes, with an initial thermal increase rate of 3 °C/min. The sintered pellets were allowed to cool naturally within the furnace.

Crystalline phase identification and analysis were performed using a Rigaku MiniFlex II X-ray diffractometer (XRD) with radiation, operating in the angular range of 20° to 80°. This analysis was essential for confirming the dominant hexagonal wurtzite structure and identifying the presence of minute CTO-rich secondary phases. Furthermore, structural integrity was assessed by determining key features such as the crystallite size (D) and micro-strain (ε), which were derived from the Full Width at Half Maximum (FWHM) of the prominent (101) diffraction peak. The physical surface morphology of the sintered ceramic pellets was examined using a Tescan Vega Scanning Electron Microscope (SEM), equipped with an Energy Dispersive X-ray (EDX) spectroscopy system. The combined SEM-EDX analysis was utilised to assess the surface structure, map the distribution of co-existing elements (Zn, O, Ca, Ti), and confirm the segregation of Ca- and Ti-rich phases at the ZnO grain boundaries (GBs) and multi-junctions. The average grain size (d) of the ZnO grains was quantified from the SEM micrographs by employing the standard lineal intercept method (Wurst, 1972). The average grain size was calculated according to Equation (1):

$$d = 1.56L/MN \quad (1)$$

Where L denotes the total length of the random lines drawn on the micrograph, M represents the image magnification, and N signifies the total number of grain boundaries intersected by the lines. The constant factor 1.56 serves as the necessary correction element used to convert the average intercept width into the average grain size. The DC electrical behaviours of the sintered ceramic pellets were characterised at room temperature using a Keithley 2410-(SCS) semiconductor characterisation system. Key varistor performance parameters were extracted directly from the current density-electric field (*J-E*) characteristics.

III. RESULTS AND DISCUSSION

A. Microstructural Evaluation

The XRD spectra presented in Figure 1 show a contrast between the pure sample and the CTO addition samples heated at 1250 °C. The XRD patterns confirmed the main phase of polycrystalline ZnO (ICDD card no. 01-080-3004), and a small peak corresponding to the CTO-rich phase (ICDD card no. 01-078-5896) in all samples. The prominent peak detected at the (101) plane is spotted as the dominant phase of the ZnO wurtzite structure. The phase of CTO concentrated at the (112) plane as the CTO content increases up to 1.0 mol%. Table 1 summarises the infinitesimal alterations in the Bragg angle and intensity shift of ZnO and CTO phases. It can be observed that the intensity of the ZnO Bragg peak (101) increased up to 186004.44 cps at 0.6 mol% of CTO, then dropped with an increasing number of additives.

With the sole exception of the (112) CTO planes, there is essentially no additional perovskite-related diffraction peak visible in the sample doped with 0.2 and 0.4 mol% CTO, suggesting that CTO is present predominantly as a single secondary phase at these low doping concentrations. As the CTO content increases to 0.6 mol%, an additional CTO-related diffraction peak at the (220) plane emerges in the XRD profile, coinciding with the observed increase in ZnO (101) intensity (Yildiz & Toplan, 2006). With further increases in CTO content to 0.8 and 1.0 mol%, the ZnO (101) intensity decreases as additional CTO-related diffraction peaks at the (103) and (224) planes appear progressively. The progressive appearance of multiple diffraction peaks (112), (220), (103), and (224) with rising CTO concentration offers definitive crystallographic proof that CTO fails to persist as a solitary secondary phase at elevated doping levels. Instead, it partitions into several coexisting CTO-rich secondary phases along grain boundaries. This doping-dependent phase progression holds critical implications for interpreting the microstructural and electrical characteristics of these doped ceramics. The decline in ZnO (101) peak intensity with increasing CTO levels arises from two synergistic factors. Initially, Ti^{4+} (0.605 Å) ions progressively replace Zn^{2+} (0.74 Å) in the ZnO lattice, causing structural distortions and strain that impair long-range crystallinity and diffraction coherence (Diallo *et al.*, 2026). Additionally, the growing proportion of CTO-rich secondary phases at grain boundaries reduces the effective ZnO crystalline volume available for diffraction. Collectively, these mechanisms diminish the overall intensity of the primary ZnO (101) peak at elevated doping concentrations. Figure 2 presents a comparison of XRD spectra with a close-up view of 2θ measurements of 35 to 37° corresponding to the ZnO (101) peak.

Table 1. The Bragg angle and intensity shift of ZnO (101) and CTO (112) planes with respect to additive compositions.

Composition (mol%)	Bragg Angle (°)		Intensity (cps)	
	ZnO (101)	CTO (112)	ZnO (101)	CTO (112)
0.0	36.20	-	154922.21	-
0.2	36.18	33.20	159106.67	1007.78
0.4	36.13	33.02	179672.22	1167.78
0.6	36.31	33.14	186004.44	1511.11
0.8	36.27	33.08	147422.22	1432.22
1.0	36.21	33.08	176790.70	1316.64

The peaks of the (110) planes clearly shifted at various angles relative to the pure ZnO sample, as shown in Figure 2. The ZnO (101) peak exhibited a subtle shift towards higher Bragg angles for the 0.6 mol% and 0.8 mol% samples. This displacement is consistent with lattice contraction driven by the substitutional exchange of larger host Zn ions by the smaller Ti ions within the ZnO lattice. This ionic mismatch introduces significant internal strain into the ZnO crystal lattice, which directly governs the resulting variations in the diffraction peak angles and intensity (Belgacem *et al.*, 2015).

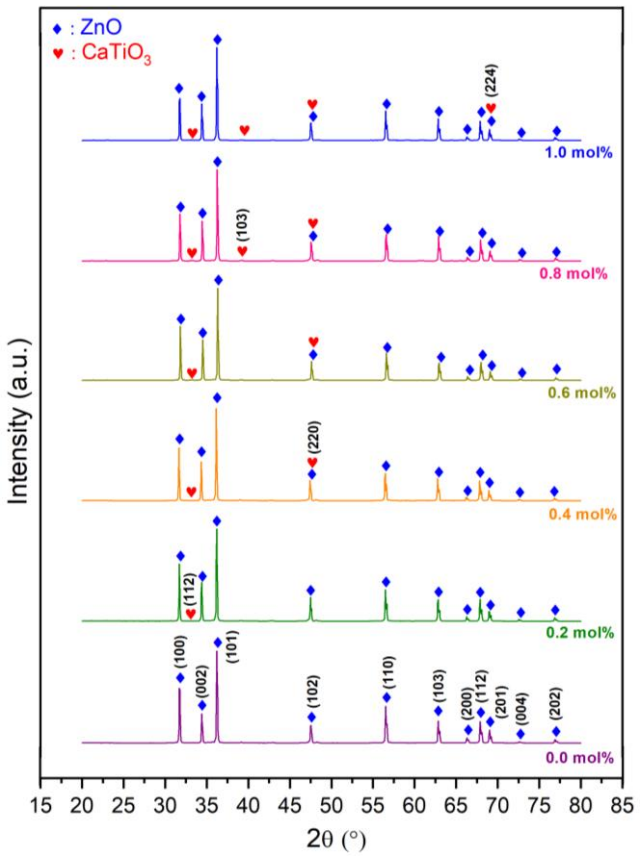

Figure 1. XRD patterns of ZnO varistor doped with different CTO contents.

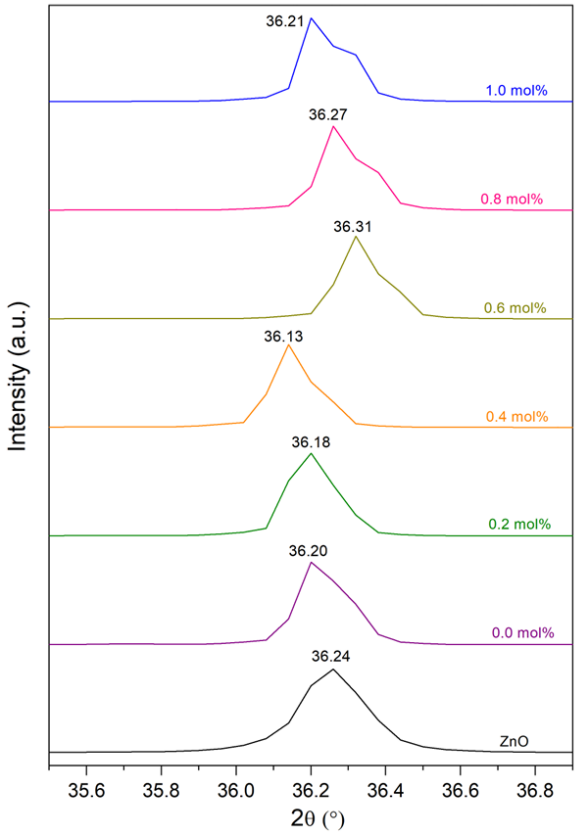

Figure 2. Expanded XRD ZnO (101) peaks in the 35 to 37° of 2θ region.

Table 2. Structural features of ZnO-based varistors prepared at various CTO concentrations.

Concentration (mol%)	FWHM, β (°)	Crystallite size, D (nm)	Micro-strain, ε (10^{-3})	d-spacing (Å)	Relative variation (%)
0.0	0.160	52.31	2.13	2.60749	0.095
0.2	0.151	55.43	2.01	2.60873	0.143
0.4	0.136	61.28	1.82	2.61185	0.263
0.6	0.141	59.46	1.87	2.60068	-0.166
0.8	0.153	54.51	2.04	2.60315	-0.071
1.0	0.159	52.58	2.12	2.60687	0.071

Table 2 records the structural features of the base varistor prepared at various CTO concentrations. The strong ionic drift of titanium ions prompts their diffusion into the ZnO lattice, consequently adjusting the overall crystalline configuration to a state of reduced interplanar spacing. This is quantitatively demonstrated by the measured d-spacing values, which exceeded 2.60068 Å for the 0.6 mol% sample and 2.60315 Å for the 0.8 mol% sample. The 0.6 mol% sample shows the strongest diffraction intensity. Beyond 0.4 mol%, crystallite size steadily decreases while micro-strain increases, hitting the smallest size and highest strain at 1.0 mol% CTO. This has been updated in the statement.

Conversely, the addition of CTO up to 0.4 mol% appears to shift the ZnO (110) peaks to the left, indicating a lower 2θ value. This study supports the reciprocal relationship between crystallite size and the full-width half-maximum (FWHM). The values of FWHM dropped from 1.60° to 0.141°, then slightly increased to 0.159° for the sample doped with 1.0 mol% CTO, indicating the lattice warping of crystalline flaws that caused the primary broadening of the XRD spectra (La Porta *et al.*, 2014). This indirect measurement justifies the inverse relationship between FWHM and crystallite size by demonstrating that the smaller crystallite size is a result of increased CTO doping concentrations. The effects of CTO addition on the internal lattice strain are concentration-dependent and non-monotonic. At low doping levels of 0.2-0.4 mol%, the preferential segregation of CTO to grain boundaries partially relieves pre-existing intrinsic stress within the ZnO lattice, resulting in a reduction of micro-strain relative to the undoped sample. However, beyond 0.4 mol%

CTO, the gradual replacements of Zn^{2+} by Ti^{4+} ions and the emergence of various CTO-rich secondary phases lead to heightened lattice inhomogeneities and structural disorder which induce the formation of internal lattice strain within the host lattice (Hassanzadeh-Tabrizi, 2023). The micro-strain for the undoped sample equals 2.13×10^{-3}. The addition of CTO into ZnO varistors indicated an alteration in micro-strain, as the value decreased until 0.4 mol% of CTO addition, then rose with further increments of CTO content. This can be attributed to the presence of inhomogeneous phases within the sample, as depicted in Figure 1, which shows the existence of two CTO phases (103) and (224).

The grain formation of ZnO varistor ceramics' surface configurations with various additive contents is illustrated in Figure 3. The SEM micrographs reveal the presence of ZnO grains, triple points, grain boundaries, and porosities, from samples sintered at 1250 °C for 90 minutes. Compact grains with barely any visible pores appeared in the sample with no CTO. In contrast, the CTO-doped ZnO varistors show some smaller grains, indicating CTO elements that are randomly distributed and become more clearly visible at a higher doping level of CTO in the ceramics. The Ca-rich phase is found clumping at multiple grain junctions, along grain borders, or at the exterior of the ZnO grains. The host grain of ZnO improves over time when titanium dioxide is introduced into the ZnO varistor system through the CTO additive (Toplan & Karakaş, 2002). The ZnO grain size for doped samples is slightly larger compared to the pristine sample, as shown in Figure 3. Figure 4 presents the elemental dispersion using X-ray mapping, and Table 3 confirms the presence of the detected elements within the ceramic samples. It is distinctly observed that the CTO is unevenly distributed within the ceramic matrix. At low doping concentrations (0.2 and 0.4 mol%), CTO is predominantly present as a single secondary phase identifiable by the (112) diffraction peak, which is consistent with the perovskite $CaTiO_3$ structure. However, at higher concentrations, CTO segregates into multiple secondary phases, as evidenced by the progressive emergence of additional diffraction peaks at the (220), (103), and (224) planes in the XRD patterns.

Table 3 EDX results of ZnO varistor doped with different CTO contents.

CTO compositions (mol%)	Energy of X-ray emitted by elements (keV)			
	Zn	O	Ca	Ti
0.0	85.20	14.80	-	-
0.2	82.24	16.76	0.54	0.47
0.4	82.22	15.50	1.11	1.16
0.6	82.89	15.85	0.62	0.64
0.8	74.79	16.65	4.07	4.50
1.0	81.87	15.64	1.12	1.36

As observed in Figure 4, all the associated elements were detected, supported by the XRD outcomes in each doping system. Zn atoms are seen surrounding all parts of the grains. Both Zn and O atoms preferentially aggregate at the grain boundaries, effectively creating trap holes that lead to an oxidised phase along the grain edges (Tian *et al.*, 2021). EDX analysis reveals the presence of Ca and Ti elements, primarily located near the multi-junctions, although some are also found on the grain surfaces in CTO-doped ceramics. In the 0.4 mol% sample, solely the (112) CTO peak remains detectable, which mirroring the 0.2 mol% case, albeit with marginally elevated intensity. At 0.6 mol% CTO, the (220) peak emerges additionally. Higher levels doping of 0.8 to 1.0 mol% yield further CTO phases at (103) and (224) planes, evidencing escalating perovskite accumulation along grain boundaries. Based on Table 3, the highest amounts of Ca and Ti are measured at 0.8 mol% CTO doping, consistent with XRD results revealing the emergence of a new CTO-rich diffraction peak at the (103) crystallographic plane. However, the increase in doping content up to 0.8 mol% appears to disrupt the ordered evolution of the grain microstructure, as indicated by qualitative SEM observations in the 0.8 mol% sample (Figure 3e). These include diminished grain boundary definition, heightened surface roughness, and evident agglomeration of secondary phase particles at grain junctions. Although SEM imaging does not quantify crystallinity directly, these morphological signatures align with and are substantiated by XRD data showing peak broadening and increased micro-strain at elevated CTO levels, collectively pointing to a gradual degradation of long-range crystalline order in the ZnO matrix.

It is often speculated that some Ti ions are substituted in the Zn lattice because the ionic radius of Ti is smaller than that of Zn, rather than aiding the development of phase segregation (Liao *et al.*, 2021). Since the ratio of Ti is greater than that of Ca at low doping concentration, Ti exerts a stronger influence on the ceramic microstructure in this regime. Therefore, at low CTO concentrations (0.2-0.4 mol%), Ti is presumed to act as a grain growth enhancer, promoting the formation of larger grains through enhanced grain boundary mobility during sintering. However, this grain-promoting effect is concentration-dependent. At higher CTO concentrations (0.8 and 1.0 mol%), the excess CTO beyond its solubility limit precipitates as secondary phase particles at the grain boundaries, as evidenced by the emergence of additional XRD peaks at the (103) and (224) planes. These secondary phase particles serve as pinning centers that hinder grain boundary motion via the classic Zener pinning effect, thereby inhibiting additional grain growth. Additionally, the accumulation of Ca-rich phases at higher doping levels further contributes to grain refinement, consistent with the findings of Hembram *et al.* (2020). Consequently, the net effect of CTO on grain size transitions from growth promotion at low concentrations to grain refinement at higher concentrations, as reflected in the average grain size values presented in Table 4.

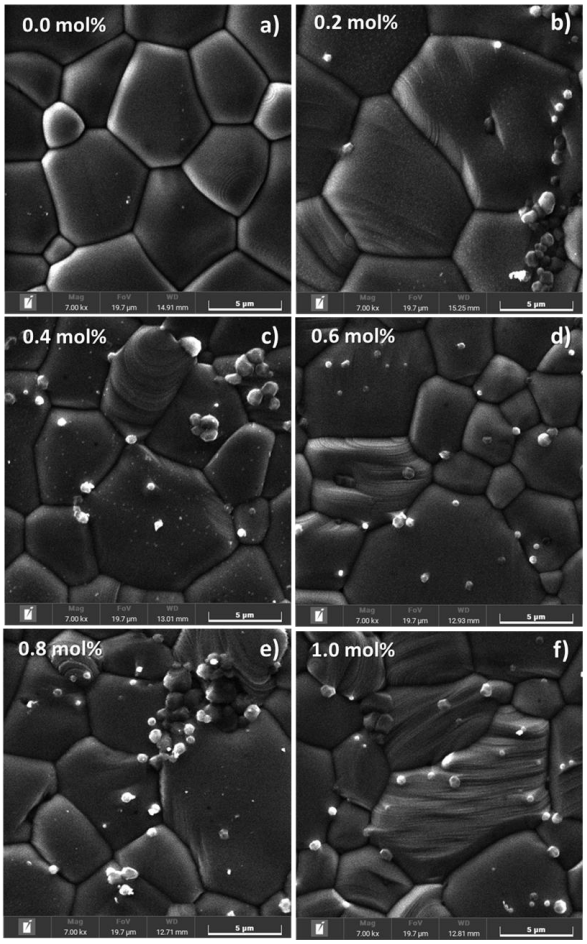

Figure 3. Electron imaging of ZnO varistors doped with different CTO contents: a) 0.0 mol%, b) 0.2 mol%, c) 0.4 mol%, d) 0.6 mol%, e) 0.8 mol%, and f) 1.0 mol%.

The CTO additive influences the growth of ZnO ceramics, as shown in Figure 3, where all samples doped with CTO exhibit somewhat larger ZnO grains, except for those doped with 0.8 and 1.0 mol% of CTO. Table 4 tabulates the relative density and average grain size of ZnO varistors doped with different CTO contents. The sample without the CTO additive has an average grain size of 9.4 μm. The addition of CTO to ZnO ceramic enhances the grain size at 0.2 mol% CTO, but with further doping content, the grain size decreases moderately, reaching 8.84 μm for the sample with 1.0 mol% CTO doping. As noted by Hembram *et al.*, CaO plays a role in preventing the enlargement of ZnO grains, thereby slowing down grain growth (Hembram *et al.*, 2020). However, doping with CTO in ZnO varistor is detrimental to the compaction process (densification), as the relative density decreases with increasing CTO content in ZnO varistor systems.

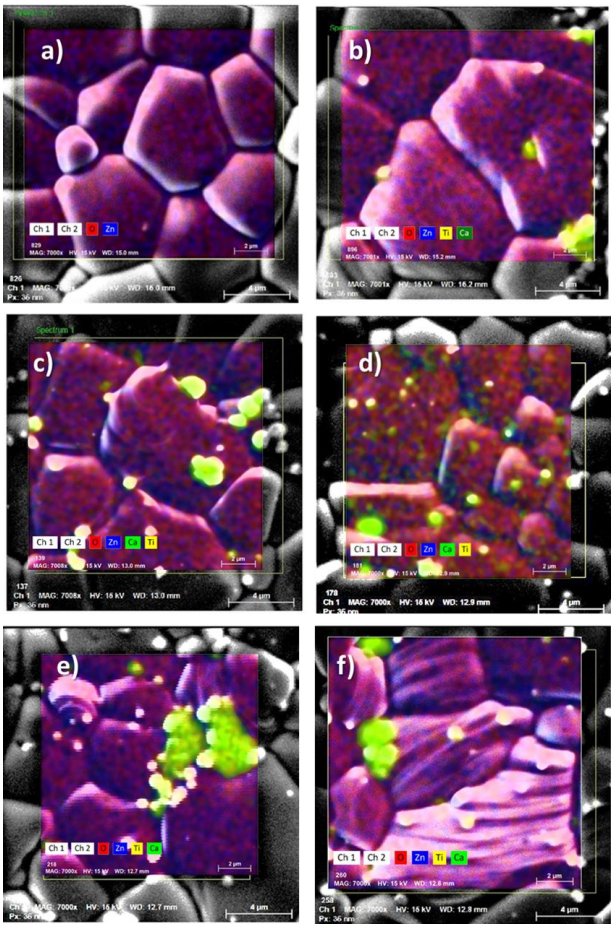

Figure 4. Spatial distribution of elements in ZnO varistors with various doping levels of CTO: a) 0.0 mol%, b) 0.2 mol%, c) 0.4 mol%, d) 0.6 mol%, e) 0.8 mol%, and f) 1.0 mol%.

Table 4. Average grain size (d), theoretical density ($P_{theoretical}$), experimental density ($P_{experimental}$), and relative density ($P_{relative}$) of ZnO varistor with different CTO doping concentrations.

CTO contents (mol%)	d (μm)	$P_{theoretical}$ (g/cm³)	$P_{experimental}$ (g/cm³)	$P_{relative}$ (%)
0.0	9.40 ± 0.42	5.680	5.677	99.95 ± 0.03
0.2	14.68 ± 1.25	5.672	5.649	99.60 ± 0.03
0.4	11.93 ± 0.36	5.664	5.641	99.59 ± 0.03
0.6	11.58 ± 0.50	5.656	5.620	99.36 ± 0.03
0.8	9.12 ± 0.91	5.648	5.508	97.52 ± 0.03
1.0	8.84 ± 0.52	5.640	5.478	97.13 ± 0.03

The plot of average grain size and relative density values against CTO doping content is shown in Figure 5. A clear decrease in relative density is observed, attributed to the presence of CaO, which has the lowest theoretical density of all varistor ingredients. However, the measured relative density remains within an acceptable range for functional varistor ceramics. For reference, conventionally sintered Bi-free ZnO varistor systems reported in the literature typically achieve relative densities in the range of 95–99%, depending on sintering conditions and additive composition (Wang *et al.*, 2021; Hembram *et al.*, 2020; Shaifudin *et al.*, 2019). The relative densities achieved in the present study, ranging from 97.13% at 1.0 mol% CTO to 99.95% for the undoped sample are aligned with, and often surpass, values reported for analogous doped systems. The observed decline in relative density at higher CTO concentrations (0.8 and 1.0 mol%) is attributed to the lower theoretical density of CaO and the increased porosity arising from secondary phase accumulation at the grain boundaries, yet the values remain above the 97% threshold that is generally regarded as indicative of well-densified varistor ceramics (Tian *et al.*, 2024).

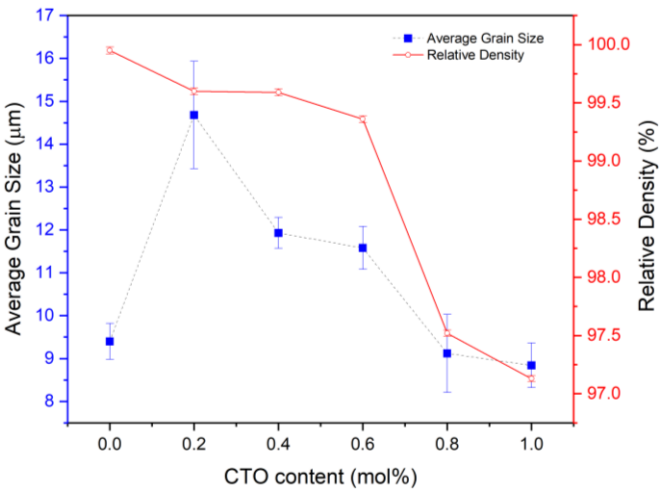

Figure 5. Average grain size and relative density with CTO content.

B. Electrical Properties Evaluation

The wide range of electrical responses observed in the ZnO varistors is determined by their doping concentration, as all these samples were sintered under fixed conditions (1250 °C for 90 min). Crucially, the surface characteristics of the ZnO ceramic intrinsically govern these resulting electrical

behaviours. Table 5 summarises key insights into the electrical characteristics of all doped ceramics, clearly demonstrating the non-ohmic behaviour of ZnO varistors. The undoped ZnO specimen, free from the specified additives, exhibited a nonlinearity coefficient α of 1.542. The behaviour of ZnO varistor samples, starting with undoped ZnO, is demonstrated in Figure 6.

The nonlinear coefficient (α) is considered the pivotal limitation parameter in varistor functionality, serving as the primary performance indicator of ZnO varistors. Higher α values indicate more efficient varistors, whereas lower α values denote subpar varistor performance (Pillai *et al.*, 2013). The ceramic doped with 1.0 mol% CTO exhibits the highest α value, with the slope nearly following a linear sequence. This positive trend clearly demonstrates that α increases with CTO doping concentration, as the integration of CTO in ZnO varistor forms a double Schottky barrier at the grain boundaries, explaining why the current does not increase linearly with the voltage of the ZnO ceramic. From Figure 7, the α value for pure ZnO is minuscule compared to the doped samples, indicating that the presence of CTO enhances α.

Table 5. Electrical characteristics of ZnO varistors with different CTO compositions.

CTO content (mol%)	α	E_B (V/mm)	J_L (μA/cm²)	Φ_B (eV)	V_{gb} (V)
0.0	1.542 ± 0.010	6.23	704.96	0.605	0.0491
0.2	2.427 ± 0.002	1.20	586.79	0.647	0.0092
0.4	2.736 ± 0.030	1.70	557.40	0.633	0.0201
0.6	2.871 ± 0.003	0.19	548.62	0.698	0.0018
0.8	3.099 ± 0.005	1.30	516.92	0.669	0.0100
1.0	3.850 ± 0.018	0.99	425.11	0.666	0.0076

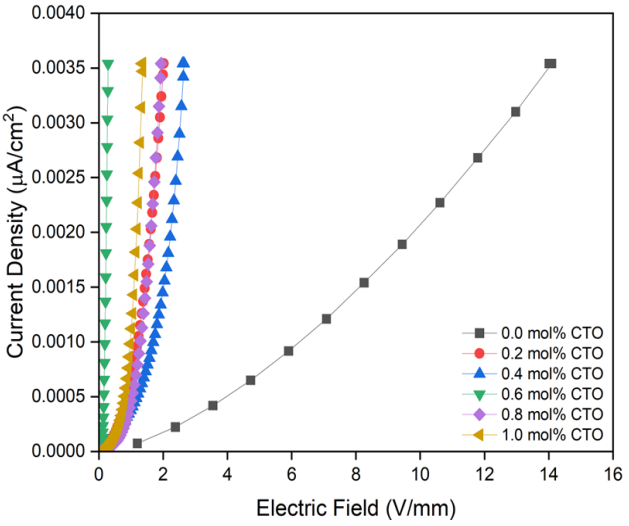

Figure 6. *J-E* curves of ZnO varistors doped with varied CTO contents.

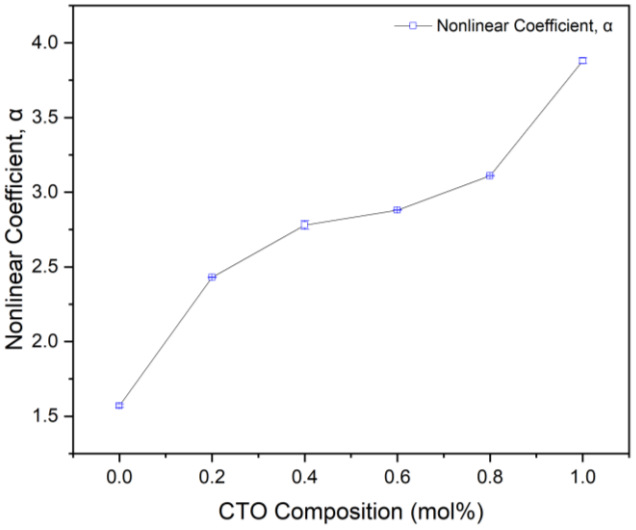

Figure 7. The nonlinear coefficients versus different CTO additive amounts.

With reference to the initial three doped ceramic samples, the breakdown field (E_B) decreased progressively from 6.23 V/mm for the undoped varistor to a minimum of 0.19 V/mm at 0.6 mol% CTO doping. This decrease is attributed to the enlargement of ZnO grains caused by the existence of grain enhancer additive, TiO_2, within the CTO doping elements (Mohammadi *et al.*, 2019). However, E_B started to rise, reaching 1.30 V/mm and 0.99 V/mm for the samples doped with 0.8 mol% and 1.0 mol% of CTO, respectively. The voltage per grain boundary (V_{gb}) is linearly related to the E_B (Leach *et al.*, 2000). The V_{gb} values reflect a similar trend to the breakdown field, spanning from 0.0018 V to 0.0100 V. Table 5 also presents the leakage current density values for different doping compositions at a fixed sintering temperature of 1250

°C. Notably, the leakage current is high for undoped ZnO ceramic, approximately 704.96 μA/cm², but decreases progressively with increasing CTO doping amounts. This improvement in α values is attributed to the formation of potential barriers that restrict the current flow due to CTO addition in ZnO varistors (Özer *et al.*, 2010).

Existing studies have proven the connection between J_L and α behaviour, and the changes in nonlinearity have been well documented. It is clear that they are inversely related—when one increases, the other decreases (Wang *et al.*, 2021). The enhancement of α triggered by increasing CTO doping amounts can be attributed to the elevation of the potential barrier height at the interface. In light of this, the measured value of Φ_B increased from 0.605 eV for the undoped ZnO varistor to 0.698 eV for the optimum value at 0.6 mol% CTO. Further addition of CTO diminished the potential barrier height; however, it remained higher than that of the undoped sample. This was attributed to the segregation of CTO that might deteriorate the varistor grain structure, as seen in the SEM micrograph (Figure 3). Despite having relatively less dense grains, the sample doped with 1.0 mol% CTO has the smallest grain size, with the most active grain boundaries, which enhance the accidental contribution to nonlinear conductivity over DSB. A comprehensive evaluation of all measured parameters reveals concentration-dependent trade-offs across the CTO doping range. Notably, the potential barrier height (Φ_B) reaches its maximum value of 0.698 eV at 0.6 mol% CTO, and relative density is better preserved at lower doping concentrations, indicating that 0.6 mol% CTO represents the optimal composition from the perspective of barrier height and densification. However, for the specific application context of low-voltage overvoltage protection, the nonlinearity coefficient (α) serves as the primary performance-determining parameter, as it directly governs the sharpness and efficiency of the switching response between the high-resistance and low-resistance states of the varistor. On this basis, the 1.0 mol% CTO-doped sample is identified as the best overall candidate for the intended application, delivering the highest α value of 3.850 and the lowest leakage current density of 425.11 μA/cm², while maintaining a breakdown voltage of 0.99 V/mm within the low-voltage operational range and a potential barrier height of 0.666 eV. The relative density of 97.13% at 1.0 mol% CTO, though lower than at other compositions, remains within the acceptable range for functional varistor ceramics as established by comparable systems in the literature.

IV. CONCLUSION

This study systematically evaluated the influence of CTO concentration (0.0–1.0 mol) on the microstructure and electrical properties of ZnO-based varistor ceramics. Low CTO levels enhanced grain growth, while higher concentrations promoted grain refinement, consistent with the distinct roles of TiO_2 and Ca-rich phases. Crystallographic analysis confirmed substitutional effects and strain dynamics. Despite the peak potential barrier height being achieved at 0.6 mol% CTO, the 1.0 mol% CTO sample is identified as the optimal composition for low-voltage protection, owing to its highest nonlinearity coefficient (α = 3.85) and lowest leakage current density (425.11 μA/cm²). Given that these parameters are the foremost indicators of varistor functionality, their optimisation at 1.0 mol% CTO outweighs the trade-offs in barrier height and densification observed at higher doping levels. The study confirms CTO as a thermally stable, effective alternative to Bi_2O_3, establishing a foundation for environmentally friendly, high-performance ZnO varistors. Future research should focus on optimising this concentration threshold by integrating other suitable additives to further enhance the absolute value of the nonlinear coefficient.

V. ACKNOWLEDGEMENT

The authors would like to thank the Ministry of Higher Education Malaysia and Universiti Malaysia Terengganu for funding the research under the Talent and Publication Enhancement-Research Grant (TAPE-RG/2022/Vot. No. 55385).

VI. REFERENCES

Belgacem, RB, Chaari, M & Matoussi, A 2015, 'Studies on structural and electrical properties of ZnO/TiO2 composite materials', *Journal of Alloys and Compounds*, vol. 651, pp. 49-58.

Diallo, SB, Khlifi, N, Fall, M & Guermazi, H 2026, 'Tunable structure–property engineering and visible-light photocatalytic performance of ZnO: TiO2 nanocomposites synthesized via a solid-state route', RSC advances, vol. 16, no. 5, pp. 4090-4106.

Fauzana, A, Azmi, B, Sabri, M, Wan Abdullah, W & Hashim, M 2013, 'Microstructural and nonlinear electrical properties of ZnO ceramics with small amount of MnO_2 dopant', *Sains Malaysiana*, vol. 42, no. 8, pp. 1139-1144.

Hassanzadeh-Tabrizi, S 2023, 'Precise calculation of crystallite size of nanomaterials: A review', *Journal of Alloys and Compounds*, p. 171914.

He, J 2019, *Metal oxide varistors: from microstructure to macro-characteristics*, John Wiley & Sons.

Hembram, K, Rao, TN, Ramakrishana, M, Srinivasa, RS & Kulkarni, AR 2020, 'Influence of CaO doping on phase, microstructure, electrical and dielectric properties of ZnO varistors', *Journal of Alloys and Compounds*, vol. 817.

Hembram, K, Rao, TN, Srinivasa, RS & Kulkarni, AR 2021, 'CaO doped ZnO–Bi2O3 varistors: Grain growth mechanism, structure and electrical properties', *Ceramics International*, vol. 47, no. 1, pp. 1229-1237.

La Porta, FA, Andres, J, Vismara, M, Graeff, CFDO, Sambrano, JR, Li, MS, Varela, JA & Longo, E 2014, 'Correlation between structural and electronic order–disorder effects and optical properties in ZnO nanocrystals', *Journal of Materials Chemistry C*, vol. 2, no. 47, pp. 10164-10174.

Lan, P, Zhao, H, Liu, W, Zhao, X, Guo, M & Liu, M 2025, 'Influence of Sintering Profiles on Point Defects in ZnO Varistors', *Ceramics International*.

Leach, C, Ling, Z & Freer, R 2000, 'The effect of sintering temperature variations on the development of electrically active interfaces in zinc oxide based varistors', *Journal of the European Ceramic Society*, vol. 20, no. 16, pp. 2759-2765.

Liao, X, Pu, Y & Zhu, D 2021, 'Synergistic effect of co-doping of nano-sized ZnO and Nb_2O_5 on the enhanced nonlinear coefficient of TiO_2 varistor with low breakdown voltage', *Journal of Alloys and Compounds*, vol. 886, p. 161170.

Lungu, MV 2023, 'Effects of dopants and processing parameters on the properties of ZnO-V_2O_5-based varistors prepared by powder metallurgy: a review', *Materials*, vol. 16, no. 10, p. 3725.

Malaoui, Y, Kharchouche, F, Sari, B & Bernik, S 2025, 'Optimisation of dopants proportions in Bi_2O_3 doped ZnO-based varistor using neural networks technique for enhanced nonlinear coefficient and performance', *Ceramics International*.

Mohammadi, R, Azis, R, Zakaria, A, Isa, N, Saat, N, Mokhtar, N & Muhammad, F 2019, 'Electrical and Microstructural Properties of ZnO-Bi_2O_3-TiO_2-Sb_2O_3-Al_2O_3-Based Varistor Ceramics Fabricated by Solution Coating Method', *Digest Journal of Nanomaterials and Biostructures*, vol. 14, no. 4, pp. 1105-1113.

Özer, İÖ, Suvaci, E & Bernik, S 2010, 'Microstructure–property relationship in textured ZnO-based varistors', *Acta Materialia*, vol. 58, no. 12, pp. 4126-4136.

Peiteado, M, De la Rubia, M, Velasco, M, Valle, F & Caballero, A 2005, 'Bi_2O_3 vaporisation from ZnO-based varistors', *Journal of the European Ceramic Society*, vol. 25, no. 9, pp. 1675-1680.

Pillai, SC, Kelly, JM, Ramesh, R & McCormack, DE 2013, 'Advances in the synthesis of ZnO nanomaterials for varistor devices', *Journal of Materials Chemistry C*, vol. 1, no. 20, pp. 3268-3281.

Prachamon, J, Sattapol, P, Chanlek, N, Putasaeng, B, Phromviyo, N, Harnchana, V, Swatsitang, E & Thongbai, P 2023, 'Significantly improved giant dielectric properties and enhanced nonlinear coefficient of Ni^{2+} doped $CaCu_3Ti_4O_{12}$/$CaTiO_3$ composites', *Heliyon*, vol. 9, no. 6.

Shahraki, MM, Daeijavad, H, Emami, AH, Abdollahi, M & Karimi, A 2019, 'An engineering design based on nano/micro-sized composite for $CaTiO_3$/$CaCu_3Ti_4O_{12}$ materials and its dielectric and non-Ohmic properties', *Ceramics International*, vol. 45, no. 17, pp. 21676-21683.

Shaifudin, MS, Ghazali, MSM, Abdullah, WRW, Kassim, S & Kamaruzzaman, WMIWM 2019, 'Microstructure and Electrical Properties of Low-Voltage Barium Titanate Doped Zinc Oxide Varistor Ceramics', *International Journal of Recent Technology and Engineering (IJRTE)*, vol. 8, no. 4, pp. 2713-2718. doi: 10.35940/ijrte.D7326.118419

Tian, T, Zheng, L, Podlogar, M, Zeng, H, Bernik, S, Xu, K, Ruan, X, Shi, X & Li, G 2021, 'Novel ultrahigh-performance ZnO-based varistor ceramics', *ACS Applied Materials & Interfaces*, vol. 13, no. 30, pp. 35924-35929.

Tian, T, Zheng, L, Bernik, S, Ruan, X & Li, G 2024, 'Influence of TiO_2 doping on the grain growth and electrical properties of ZnO–Cr_2O_3-based varistor ceramics', Journal of Alloys and Compounds, vol. 1008, p. 176657.

Toplan, HÖ & Karakaş, Y 2002, 'Grain growth in TiO_2-added ZnO–Bi_2O_3–CoO–MnO ceramics prepared by chemical processing', *Ceramics International*, vol. 28, no. 8, pp. 911-915.

Wang, H, Zhao, H, Liang, W, Fan, S & Kang, J 2021, 'Effect of sintering process on the electrical properties and microstructure of Ca-doped ZnO varistor ceramics', *Materials Science in Semiconductor Processing*, vol. 133, p. 105880.

Wurst, J 1972, 'Linear intercept technique for measuring grain size in two-phase polycrystalline ceramics', *Journal of the American Ceramic Society*, vol. 55, p. 109.

Yang, L, Ren, B, Liu, J, Cao, W, Xu, B, Zhao, N, Gou, C & Zhang, X 2025, 'Preparation and electrical properties of Er_2O_3-doped ZnO varistors with low leakage current and high nonlinear coefficient', *Ceramics International*.

Yildiz, K & Toplan, H 2006, 'Densification and grain growth of SiO_2-doped ZnO. Ceramics International.